PHYSICAL REVIEW D **92,** 032007 (2015)

Measurement of the proton-air cross section with Telescope Array's Middle Drum detector and surface array in hybrid mode

R. U. Abbasi,[1*] M. Abe,[2] T. Abu-Zayyad,[1] M. Allen,[1] R. Azuma,[3] E. Barcikowski,[1] J. W. Belz,[1] D. R. Bergman,[1] S. A. Blake,[1] R. Cady,[1] M. J. Chae,[4] B. G. Cheon,[5] J. Chiba,[6] M. Chikawa,[7] W. R. Cho,[8] T. Fujii,[9] M. Fukushima,[9,10] T. Goto,[11] W. Hanlon,[1] Y. Hayashi,[11] N. Hayashida,[12] K. Hibino,[12] K. Honda,[13] D. Ikeda,[9] N. Inoue,[2] T. Ishii,[13] R. Ishimori,[3] H. Ito,[14] D. Ivanov,[1] C. C. H. Jui,[1] K. Kadota,[15] F. Kakimoto,[3] O. Kalashev,[16] K. Kasahara,[17] H. Kawai,[18] S. Kawakami,[11] S. Kawana,[2] K. Kawata,[9] E. Kido,[9] H. B. Kim,[5] J. H. Kim,[1] J. H. Kim,[19] S. Kitamura,[3] Y. Kitamura,[3] V. Kuzmin,[16] Y. J. Kwon,[8] J. Lan,[1] S. I. Lim,[4] J. P. Lundquist,[1] K. Machida,[13] K. Martens,[10] T. Matsuda,[20] T. Matsuyama,[11] J. N. Matthews,[1] M. Minamino,[11] Y. Mukai,[13] I. Myers,[1] K. Nagasawa,[2] S. Nagataki,[14] T. Nakamura,[21] T. Nonaka,[9] A. Nozato,[7] S. Ogio,[11] J. Ogura,[3] M. Ohnishi,[9] H. Ohoka,[9] K. Oki,[9] T. Okuda,[22] M. Ono,[23] A. Oshima,[24] S. Ozawa,[17] I. H. Park,[25] M. S. Pshirkov,[16,26] D. C. Rodriguez,[1] G. Rubtsov,[16] D. Ryu,[19] H. Sagawa,[9] N. Sakurai,[11] L. M. Scott,[27] P. D. Shah,[1] F. Shibata,[13] T. Shibata,[9] H. Shimodaira,[9] B. K. Shin,[5] H. S. Shin,[9] J. D. Smith,[1] P. Sokolsky,[1] R. W. Springer,[1] B. T. Stokes,[1] S. R. Stratton,[1,27] T. A. Stroman,[1] T. Suzawa,[2] M. Takamura,[6] M. Takeda,[9] R. Takeishi,[9] A. Taketa,[28] M. Takita,[9] Y. Tameda,[12] H. Tanaka,[11] K. Tanaka,[29] M. Tanaka,[20] S. B. Thomas,[1] G. B. Thomson,[1] P. Tinyakov,[30,16] I. Tkachev,[16] H. Tokuno,[3] T. Tomida,[31] S. Troitsky,[16] Y. Tsunesada,[3] K. Tsutsumi,[3] Y. Uchihori,[32] S. Udo,[12] F. Urban,[30] G. Vasiloff,[1] T. Wong,[1] R. Yamane,[11] H. Yamaoka,[20] K. Yamazaki,[28] J. Yang,[4] K. Yashiro,[6] Y. Yoneda,[11] S. Yoshida,[18] H. Yoshii,[33] R. Zollinger,[1] and Z. Zundel[1]

(Telescope Array Collaboration)

[1]*High Energy Astrophysics Institute and Department of Physics and Astronomy, University of Utah, Salt Lake City, Utah, USA*
[2]*The Graduate School of Science and Engineering, Saitama University, Saitama, Saitama, Japan*
[3]*Graduate School of Science and Engineering, Tokyo Institute of Technology, Meguro, Tokyo, Japan*
[4]*Department of Physics and Institute for the Early Universe, Ewha Womans University, Seodaaemun-gu, Seoul, Korea*
[5]*Department of Physics and The Research Institute of Natural Science, Hanyang University, Seongdong-gu, Seoul, Korea*
[6]*Department of Physics, Tokyo University of Science, Noda, Chiba, Japan*
[7]*Department of Physics, Kinki University, Higashi Osaka, Osaka, Japan*
[8]*Department of Physics, Yonsei University, Seodaemun-gu, Seoul, Korea*
[9]*Institute for Cosmic Ray Research, University of Tokyo, Kashiwa, Chiba, Japan*
[10]*Kavli Institute for the Physics and Mathematics of the Universe (WPI), Todai Institutes for Advanced Study, The University of Tokyo, Kashiwa, Chiba, Japan*
[11]*Graduate School of Science, Osaka City University, Osaka, Osaka, Japan*
[12]*Faculty of Engineering, Kanagawa University, Yokohama, Kanagawa, Japan*
[13]*Interdisciplinary Graduate School of Medicine and Engineering, University of Yamanashi, Kofu, Yamanashi, Japan*
[14]*Astrophysical Big Bang Laboratory, RIKEN, Wako, Saitama, Japan*
[15]*Department of Physics, Tokyo City University, Setagaya-ku, Tokyo, Japan*
[16]*Institute for Nuclear Research of the Russian Academy of Sciences, Moscow, Russia*
[17]*Advanced Research Institute for Science and Engineering, Waseda University, Shinjuku-ku, Tokyo, Japan*
[18]*Department of Physics, Chiba University, Chiba, Chiba, Japan*
[19]*Department of Physics, School of Natural Sciences, Ulsan National Institute of Science and Technology, UNIST-gil, Ulsan, Korea*
[20]*Institute of Particle and Nuclear Studies, KEK, Tsukuba, Ibaraki, Japan*
[21]*Faculty of Science, Kochi University, Kochi, Kochi, Japan*
[22]*Department of Physical Sciences, Ritsumeikan University, Kusatsu, Shiga, Japan*
[23]*Department of Physics, Kyushu University, Fukuoka, Fukuoka, Japan*
[24]*Engineering Science Laboratory, Chubu University, Kasugai, Aichi, Japan*
[25]*Department of Physics, Sungkyunkwan University, Jang-an-gu, Suwon, Korea*
[26]*Sternberg Astronomical Institute, Moscow M.V. Lomonosov State University, Moscow, Russia*
[27]*Department of Physics and Astronomy, Rutgers University – The State University of New Jersey, Piscataway, New Jersey, USA*
[28]*Earthquake Research Institute, University of Tokyo, Bunkyo-ku, Tokyo, Japan*
[29]*Graduate School of Information Sciences, Hiroshima City University, Hiroshima, Hiroshima, Japan*
[30]*Service de Physique Théorique, Université Libre de Bruxelles, Brussels, Belgium*

[31]*Department of Computer Science and Engineering, Shinshu University, Nagano, Nagano, Japan*
[32]*National Institute of Radiological Science, Chiba, Chiba, Japan*
[33]*Department of Physics, Ehime University, Matsuyama, Ehime, Japan*
(Received 7 May 2015; published 25 August 2015; corrected 14 September 2015)

In this work we are reporting on the measurement of the proton-air inelastic cross section $\sigma^{\text{inel}}_{p-\text{air}}$ using the Telescope Array detector. Based on the measurement of the $\sigma^{\text{inel}}_{p-\text{air}}$, the proton-proton cross section σ_{p-p} value is also determined at $\sqrt{s} = 95^{+5}_{-8}$ TeV. Detecting cosmic ray events at ultrahigh energies with the Telescope Array enables us to study this fundamental parameter that we are otherwise unable to access with particle accelerators. The data used in this report are the hybrid events observed by the Middle Drum fluorescence detector together with the surface array detector collected over five years. The value of the $\sigma^{\text{inel}}_{p-\text{air}}$ is found to be equal to $567.0 \pm 70.5[\text{Stat}]^{+29}_{-25}[\text{Sys}]$ mb. The total proton-proton cross section is subsequently inferred from Glauber formalism and the Block, Halzen and Stanev QCD inspired fit and is found to be equal to $170^{+48}_{-44}[\text{Stat}]^{+19}_{-17}[\text{Sys}]$ mb.

DOI: 10.1103/PhysRevD.92.032007 PACS numbers: 13.85.Lg, 13.85.Tp

I. INTRODUCTION

Measuring the proton-air inelastic cross section $\sigma^{\text{inel}}_{p-\text{air}}$ from cosmic rays at ultrahigh energies allows us to achieve knowledge of a fundamental particle property that we are unable to attain with measurements at current accelerators. The highest proton-proton center of mass energy is currently ~14 TeV and was attained by the Large Hadron Collider (LHC). However, ultra-high-energy cosmic ray (UHECR) experiments have been reporting on the proton-air inelastic cross section, starting with the Fly's Eye in 1984 at $\sqrt{s} =$ 30 TeV [1] and ending with the most recent result of the Auger experiment at $\sqrt{s} = 57$ TeV in 2012 [2].

The current high-energy models agree in their predictions of rising proton-air cross section with energy. The high- energy models are in reasonable agreement at lower energies, below 10^{15} eV, where they are tuned to measurements of multiparticle production provided by particle accelerators. However the high-energy models diverge in describing fundamental parameters such as hadronic cross sections, elasticity, and secondary particle multiplicity above 1 PeV where the models rely solely on theoretical expectations [3]. Studying the energy dependence of the proton-air cross section is important in constraining the extrapolation of the hadronic models to high energy.

Detecting UHECR showers provides the opportunity to study fundamental particle properties. Optimally, to measure the $\sigma^{\text{inel}}_{p-\text{air}}$ directly, we observe the first point of the proton-air interaction slant depth X_1 and fit the distribution of X_1 to recover the interaction length $\lambda_{p-\text{air}}$. However, since the observation of the first point of interaction to obtain the nucleon-air cross section is not feasible, the inelastic proton-air cross section is calculated using the distribution of the observed shower maximum X_{max}. $\lambda_{p-\text{air}}$ and consequently $\sigma^{\text{inel}}_{p-\text{air}}$, are derived from the X_{max} distribution's exponential tail.

*Corresponding author.
rasha@cosmic.utah.edu

In this work, we report on the measurement of the proton-air inelastic cross section $\sigma^{\text{inel}}_{p-\text{air}}$ using the Telescope Array's Middle Drum detector together with the surface array detector (MD-SD) in hybrid mode data [4]. The method used in this calculation is "the K-factor method," where the underlying assumption is a proportionality between the tail of the X_{max} distribution and X_1. Details of the method, the result, and the systematics of the measurement are presented in this work. In addition, the Telescope Array proton-air inelastic cross section is compared to previous results. Furthermore, the proton-proton cross section σ_{p-p} is calculated using Glauber theory together with the Block, Halzen, and Stanev (BHS) QCD-inspired fit ([5–8]). The proton-proton cross section is also compared to previous σ_{p-p} experimental results. Finally, we discuss the summary and the outlook.

II. DATA TRIGGER, RECONSTRUCTION, AND SELECTION

The data used in this analysis are collected by the Telescope Array (TA) detector located in the southwestern desert of the State of Utah. TA is an UHECR detector composed of three fluorescence detector (FD) sites and the surface detector array (SD) [9] as shown in Fig. 1. The SD array occupying 700 km^2 is bounded by the FDs. The northernmost FD is referred to as Middle Drum (MD), while the other two southern FDs are named Black Rock Mesa (BRM) and Long Ridge (LR) [10]. Moreover, a central laser facility to monitor the atmosphere and calibrate the detector is deployed in the middle of the detector and is located equidistant from the three FDs.

The two southernmost detectors, LR and BRM, consist of 12 telescopes each, while the MD detector separated from the northern edge of the SD by 10 km consists of 14 telescopes each of which uses a 5.1 m^2 spherical mirror. The fluorescence light from each mirror is connected to a camera containing 256 photomultiplier tubes (PMTs) tightly spaced. Seven of the 14 mirrors view 3°–17° in

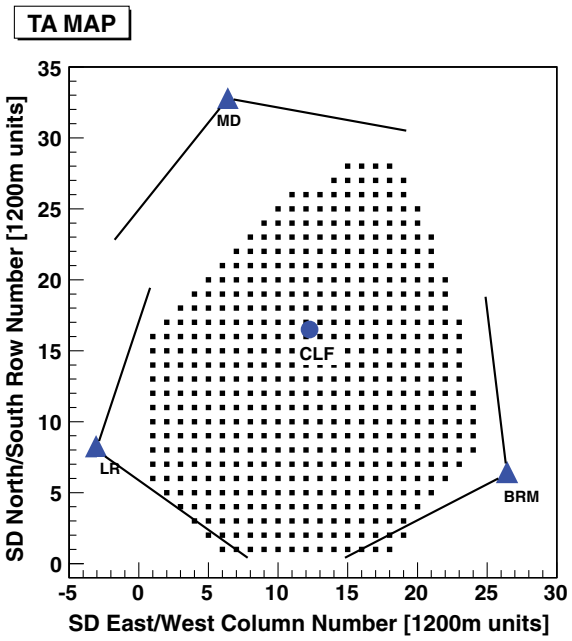

FIG. 1 (color online). The Telescope Array detector configuration. The filled squares are the 507 SD scintillators on a 1.2 km grid. The SD scintillators are enclosed by three fluorescent detectors shown in filled triangles together with their field of view in solid lines. The northernmost fluorescence detector is called Middle Drum while the southern fluorescence detectors are referred to as Black Rock Mesa and Long Ridge. The filled circle in the middle equally spaced from the three fluorescence detectors is the central laser facility used for atmospheric monitoring and detector calibration.

elevation while the rest view 17°–31°, with a total azimuth of 112° between southwest and southeast. On the other hand, the SD is composed of 507 scintillation counters each 3 m^2 in area. The SD scintillation counters are spaced on a 1.2 km grid.

The data used in this analysis consists of MD-SD hybrid events. The MD and SD trigger independently. Off-line, a hybrid data set is formed by time-matching the events from the two detectors. In the monocular mode, an event trigger is recorded by the SD when three adjacent SDs observe a signal greater than 3 minimum ionizing particles within 8 μs. When a trigger occurs, the signals from all the SDs within ± 32 μs with amplitude greater than 0.3 minimum ionizing particle are also recorded. Moreover, a telescope event trigger for the MD is recorded when two subclusters of the 256 PMT cluster triggered within 25 μs. Here a subcluster is defined as a (4×4) 16 PMTs within the 256 PMT cluster. Each subcluster reports a trigger when three tubes in that subcluster trigger within 25 μs, two of which are adjacent. Finally, multiple telescope event triggers within 100 μs would be combined into a single MD event.

Events detected by both detectors (MD and SD) within 2 μs are combined into one hybrid event. The combined data set with MD and SD time-matched events are then reprocessed using information from both detectors. The FD overlooking the sky above the SD array provides the longitudinal profile of the shower. Meanwhile, the SD provides the event shower core, particle density, and hence improves the geometrical reconstruction significantly. Reference [4] describes the detector monocular and hybrid reconstructions of the triggered events in more detail.

To achieve the best $X_{\max}$ resolution, a pattern recognition technique was applied which selected events with a well-defined peak in the fluorescence light profile. This technique is described more completely in Reference [4]. Briefly, each shower profile's shape was approximated by a set of right triangles, and a set of cuts on the properties of these triangles was used to reject $X_{\max}$ events with a "flat" profile or an indistinct peak. As shown in Reference [4], data to Monte Carlo comparison studies showed good agreement in basic air shower distributions such as zenith angle, azimuthal angle, and impact parameter after these pattern recognition cuts were applied.

The data used in this analysis is the MD-SD hybrid events collected between May 2008 and May 2013. After applying the pattern recognition cuts to the data we are left with 439 events. The energy range for this data set is between $10^{18.3}$ and $10^{19.3}$ eV. With an average energy of $10^{18.68}$ eV, this is equivalent to a center of mass energy of $\sqrt{s} = 95$ TeV. Finally, the $X_{\max}$ resolution of this data set achieved after applying the pattern recognition cuts is ~ 23 g/cm^2 [4].

III. ANALYSIS

In this paper we determine the value of $\sigma^{\text{inel}}_{p-\text{air}}$ using the K-factor method. This method infers the attenuation length and hence the cross section value from the exponential tail of the $X_{\max}$ distribution. This is assuming that the tail of the $X_{\max}$ distribution is comprised of the most penetrating/lighter particles (protons). The tail of the $X_{\max}$ distribution is fit to the exponential $\exp(\frac{-X_{\max}}{\Lambda_m})$, where Λ_m is the attenuation length. Λ_m is proportional to the interaction length $\lambda_{p-\text{air}}$:

$$\Lambda_m = K\lambda_{p-\text{air}} = K\frac{14.45 m_p}{\sigma^{\text{inel}}_{p-\text{air}}}, \quad (1)$$

where K is dependent on the shower evolution model. The departure of K from unity depends on the pion inelastic cross section and on the inclusive proton and pion cross sections with the light nuclear atmospheric target [7].

In order to determine K to derive the interaction length $\lambda_{p-\text{air}}$ from the slope of $X_{\max}$ distribution Λ_m, we carried out simulation studies using the one-dimensional air shower Monte Carlo program CONEX4.37 ([11–13]). The CONEX program uses a hybrid air shower calculation for the high-energy part of the shower, and a numerical solution of the cascade equations for the low-energy part of the shower. This hybrid approach of simulating the cosmic ray showers enables CONEX to be very efficient. Using CONEX allows

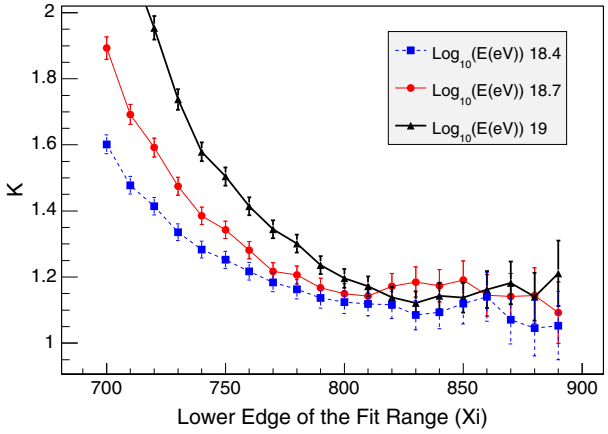

FIG. 2 (color online). The value of K vs the lower edge in the fit range X_i to the tail of the $X_{\max}$ distribution for several data sets $10^{18.4}$, $10^{18.7}$, and 10^{19} eV simulated using CONEX with the high-energy model QGSJETII.4. Each data set contains 10 000 simulated events.

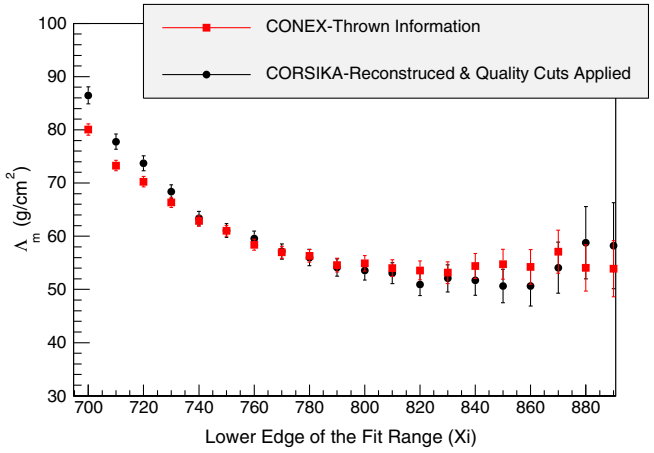

FIG. 3 (color online). Λ_m (g/cm^2) vs the lower edge in the fit range X_i to the tail of the $X_{\max}$ distribution at an energy range of $10^{18.3}$–$10^{19.3}$ eV. The value of Λ_m is calculated using CONEX with the high-energy model QGSJETII.4 (square markers). These events were not propagated through the detector. In addition, the value of Λ_m is also calculated using CORSIKA (circle markers). These events successfully survived the pattern recognition cuts after they were successfully detected and reconstructed.

us to simulate large number of showers in a very reasonable time scale. It is worth noting that the shower parameters obtained with CONEX are consistent with that obtained with CORISKA [11].

Using CONEX the value of K is determined by simulating 10 000 events for each of several energy bins for data between $10^{18.3}$ and $10^{19.3}$ eV. The value of K is calculated for each high-energy model for each energy bin by obtaining the values of Λ_m and $\lambda_{p-\text{air}}$ for that model. The value of Λ_m and therefore K for each of the data sets is impacted by the choice of the lower edge of the fit range X_i. This dependence is shown in Fig. 2.

It is essential that a consistent procedure be used to determine the X_i and consequently the value of K for the shower simulations and the observed data. We find from the data that $X_i = \langle X_{\max} \rangle + 40$ g/cm^2 is the minimum stable value of X_i, maximizing the number of events in the tail of the distribution and consequently the statistical power of the measurement. The same relative shift distribution is later used in the simulations.

It is also important to note that in addition to CONEX we have also used CORSIKA [14]. CORSIKA is used here to simulate three-dimensional cosmic ray showers. In the simulation process these showers are thinned in order to reduce the CPU time, and then dethinned in an attempt to restore lost information [15]. These showers are then propagated through the FD and the SD part of the TA detector. The showers that successfully pass the trigger of the detector are then reconstructed, after which the pattern recognition event selection are applied. The value of Λ_m is then determined and, as shown in Fig. 3, is found to be consistent with that obtained with CONEX (shower simulation not propagated through the detector) particularly around the selected choice of $X_i = \langle X_{\max} \rangle + 40$ g/cm^2. This effect will also be discussed in Sec. IV.

The value of K is calculated for each simulated data set between the energies of $10^{18.3}$ and $10^{19.3}$. Figure 4 shows K vs Log$_{10}$ (E(eV)). Note that we have chosen to display QGSJETII.4 as an example. The value of K is then established by fitting the points from Fig. 4 to a constant. Table I summarizes the high-energy models used, the value of K obtained for these models. It is also worth mentioning that the K value was also calculated with QGSJETII.3 and was obtained from this model to be consistent with that determined from QGSJETII.4 within the statistical fluctuations. Note that the stability of K around the average shown in Fig. 4 shows that K is independent of energy and

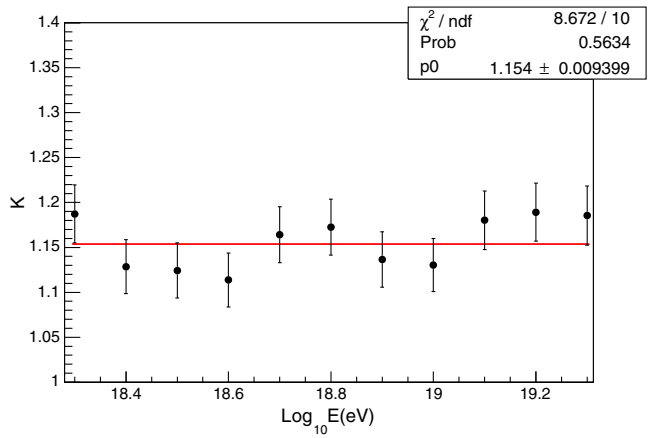

FIG. 4 (color online). The value of K obtained vs energy in Log$_{10}$(eV) for simulated data sets using CONEX with the high-energy model QGSJETII.4, for the energy range of the data, between $10^{18.3}$ and $10^{19.3}$ eV.

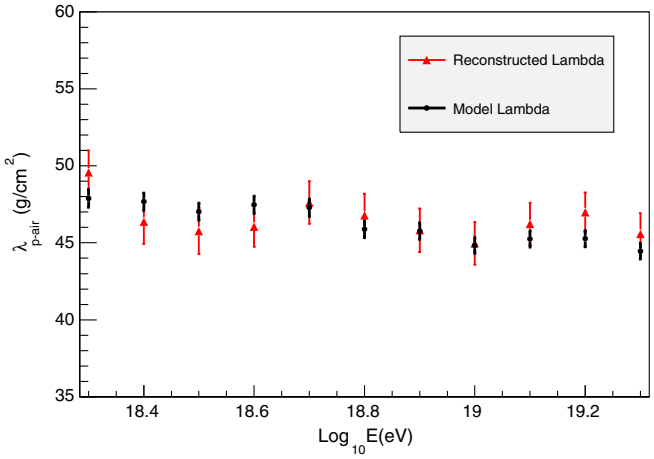

FIG. 5 (color online). The proton-air interaction length $\lambda_{p-\mathrm{air}}$ in g/cm^2 vs energy in $\mathrm{Log}_{10}(\mathrm{eV})$ for the simulated data sets using CONEX with the high-energy model QGSJETII.4, for the energy range of the data, between $10^{18.3}$ and $10^{19.3}$ eV. The circle points are the $\lambda_{p-\mathrm{air}}$ values obtained from the X_1 distribution. Triangle points are the ones determined from reconstructing the $\lambda_{p-\mathrm{air}}$ values using the K-factor method.

justifies the use of a single average value over the range of interest.

To confirm that the value of K obtained is valid to reproduce the interaction length of the model, a plot of $\lambda_{p-\mathrm{air}}$ vs $\mathrm{Log}_{10}(\mathrm{E(eV)})$ is shown in Fig. 5. Each point here represents 10 000 simulated data sets at that energy. The circle markers are the $\lambda_{p-\mathrm{air}}$ obtained from the X_1 distributions from the model, while the triangle markers are the $\lambda_{p-\mathrm{air}}$ obtained from reconstruction using the K-factor method. Figure 5 shows that using the K-factor method does indeed reconstruct the expected values of the $\lambda_{p-\mathrm{air}}$ for these simulations. This ensures that the value of K obtained in this study describe the value of K of the high-energy models correctly.

The K-factor determined in the procedure described above is dependent on the hadronic interaction model used in the air shower Monte Carlo simulation. The high-energy models used in this study are QGSJETII.4 [16], QGSJET01 [17], SIBYLL [18], and EPOS-LHC [19]. The resultant values of K determined for these models are summarized in Table I.

TABLE I. The value of K obtained for each of the high-energy models. Each K listed is the single average value of K over the energy range of $10^{18.3}$–$10^{19.3}$. Note that the values of K shows a ~3% model uncertainty.

Model	K
QGSJETII.4	1.15 ± 0.01
QGSJET01	1.22 ± 0.01
SIBYLL	1.18 ± 0.01
EPOS-LHC	1.19 ± 0.01

The first measurement of the proton-air cross section using UHECR was performed by the Fly's Eye experiment, which used a calculated value of $K = 1.6$ and obtained $\sigma^{\mathrm{inel}}_{p-\mathrm{air}} = 530 \pm 66$ mb [1]. Following the Fly's Eye result, the calculated values of K which appeared in the literature showed a continuous decrease as full Monte Carlo simulations came into use. By 2000, after the development of modern high-energy hadronic models, the reported K values still differed by approximately 7% [20]. Since then, as shown in Table I, more complete hadronic shower simulations have converged on a smaller value of $K = 1.2$, with a model uncertainty of approximately 3%. Using this lower K value, the Fly's Eye cross section may be updated to 392 ± 49 mb.

IV. PROTON-AIR CROSS SECTION

The data used in this analysis is the Telescope Array Middle Drum-Surface Detector hybrid events discussed in detail in Sec. II. Figure 6 shows the X_{max} distribution together with the exponential unbinned maximum likelihood fit to the tail between 790 and 1000 g/cm^2, the Λ_m value from the fit is found to be $(50.47 \pm 6.26[\mathrm{Stat}])$ g/cm^2.

Consecutively the value of $\sigma^{\mathrm{inel}}_{p-\mathrm{air}}$ is determined where $\sigma^{\mathrm{inel}}_{p-\mathrm{air}} = K \times 24,160/\Lambda_m$ mb using Eq. (1). The K values used are the ones calculated and summarized in the previous section in Table I. Accordingly the values of $\sigma^{\mathrm{inel}}_{p-\mathrm{air}}$ for all the considered hadronic interaction models are determined and tabulated in Table II. The final value of the proton-air cross inelastic section reported by the Telescope Array collaboration is the average value of the $\sigma^{\mathrm{inel}}_{p-\mathrm{air}}$ obtained by the high-energy models QGJSETII.4, QGSJET01, SIBYLL, and EPOS-LHC and is found to be equal to $(567.0 \pm 70.5[\mathrm{Stat}])$ mb.

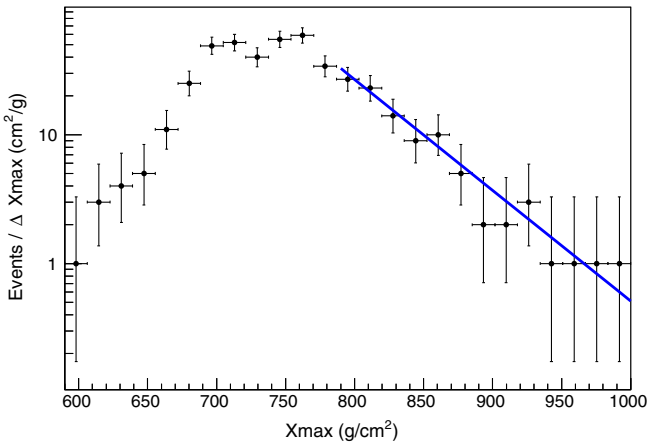

FIG. 6 (color online). The number of events per X_{max} bin (ΔX_{max}) vs X_{max} g/cm^2 for the Telescope Array data with the energy between $10^{18.3}$ and $10^{19.3}$ eV. The line is the exponential fit to the slope.

TABLE II. The high-energy model vs the $\sigma^{\rm inel}_{p-{\rm air}}$ in mb obtained for that high-energy model.

Model	$\sigma^{\rm inel}_{p-{\rm air}} \pm$ [Stat] mb
QGSJETII.4	550.3 ± 68.5
QGSJET01	583.7 ± 72.6
SIBYLL	564.6 ± 70.2
EPOS-LHC	569.4 ± 70.8

In order to quantify the systematic uncertainties on the proton-air cross section obtained using the K-factor method a few different checks were applied. First, the systematic value from the hadronic interaction model dependence of the $\sigma^{\rm inel}_{p-{\rm air}}$ value is calculated to be the maximum difference between the $\sigma^{\rm inel}_{p-{\rm air}}$ value determined from the various tested models and the average value obtained from these models. The systematic uncertainty from the model dependence is found to be (± 17) mb.

In addition, the systematic error in $\sigma^{\rm inel}_{p-{\rm air}}$ from the systematic error in Λ_m is also calculated. The data is divided in halves based on the zenith angle of the events, the distance of the shower using the impact parameter, and finally the energy of the events. The attenuation lengths resulting from all these subsets are consistent within the statistical fluctuations. In the case of the energy dependence, below the median of $10^{18.63}$ eV $\Lambda_m = 55.7 \pm 10.1$, and above the median $\Lambda_m = 45.5 \pm 7.7$.

Moreover, the systematic effect of possible energy dependent bias in the $X_{\rm max}$ distribution was studied. This is done by shifting the values of $X_{\rm max}$ by their elongation rate prior to fitting. The value of Λ_m is calculated and the systematic effect from a possible energy bias was found to be negligible.

The next check is calculating the systematic uncertainty that originates from the detector bias. This includes the bias that occurs from detecting the events, reconstructing the events, and applying the needed cuts to the events. This check is investigated by comparing the result of the attenuation length Λ_m of the simulated shower thrown without any detector effects to the attenuation length obtained from a three-dimensional shower simulation using CORSIKA propagated through the detector and reconstructed successfully including the pattern recognition cuts. As shown in Fig. 3, the value of Λ_m was found to be consistent, for all the high-energy models, between the thrown events and the reconstructed events with pattern recognition applied. Therefore, the detector bias systematic effect on the Λ_m value is negligible.

In addition, a fraction of the high-energy cosmic rays detected and used in this study are possibly photons. Such photons may accompany the cosmic rays by some scenarios explaining the origin of UHECR sources. In addition, a flux of photons is also expected from the interaction of cosmic rays with energies above 4×10^{19} eV with the microwave background radiation producing the Greisen-Zatsepin-Kuzmin process [21,22]. There have been several studies placing an upper limit on the integral flux and the fraction of the primary cosmic ray photons for energies greater than 10^{18} eV [23–25]. In this study, the lowest derived limit on the photon fraction is used and is $<1\%$ [26]. The systematic contribution from the photons is found to be $+23$ mb.

The result of the proton-air cross section from this work so far assumes, with high-energy model simulations, a pure protonic cosmic ray composition. Regardless of what conclusion one makes about the composition of the data [4,27], the result on the proton-air cross section from this work remains the same. However, the systematic effect of the presence of other elements in the data beside proton is also studied. This includes iron, helium, and CNO. Note that the maximum systematic contribution from these elements was found to be from helium (deepest $X_{\rm max}$ distribution). Hence, It is the contribution that is reported in this study. A contribution of 10%, 20%, and 50% from helium and the systematic error associated with such contribution is reported. For a 10% contribution the systematic effect is calculated to be -9 mb. Meanwhile, for a 20% and 50% contribution the systematic effect is determined to be -18 mb and -42 mb respectively. The final systematic value, conservatively assuming a 20% Helium contamination, is calculated by adding in quadrature the systematic values and is found to be $(-25, +29)$ mb. Table III summarizes the systematic checks for the proton-air cross section, including the final systematic value.

We summarize the result of the our proton-air cross section obtained using the K-factor method described previously together with the systematic checks obtained to be equal to

$$\sigma^{\rm inel}_{p-{\rm air}} = 567.0 \pm 70.5[{\rm Stat}]^{+29}_{-25}[{\rm Sys}]\ {\rm mb}. \qquad (2)$$

This is obtained at an average energy of $10^{18.68}$ eV. The result of the proton-air cross section is then compared to the results obtained from various experimental results ([1,2,28–34]) Fig. 7. In addition, the experimental results of the high-energy models (QGSJETII.4, QGSJET01, SIBYLL, EPOS-LHC) cross section predictions are also

TABLE III. The systematic source vs the systematic values of that source.

Systematic source	Systematics (mb)
Model dependence	(± 17)
10% Helium	-9
20% Helium	-18
50% Helium	-42
Gamma	$+23$
Summary (20% Helium)	$(-25, +29)$

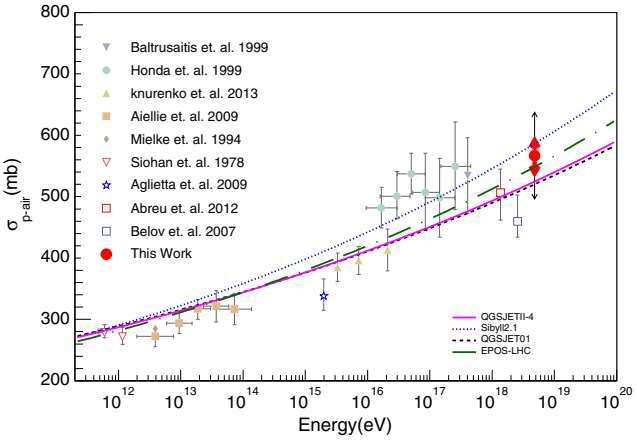

FIG. 7 (color online). The proton-air cross section result of this work, including the statistical (outer/thinner) and systematic (inner/thicker) error bar. The result of this work is shown in comparison to other experimental results [1,2,28–34]. In addition, the high-energy models (QGSJETII.4, QGSJET01, SIBYLL, EPOS-LHC) cross section predictions are also shown by solid line, fine dashed line, dotted line, and dashed line consecutively.

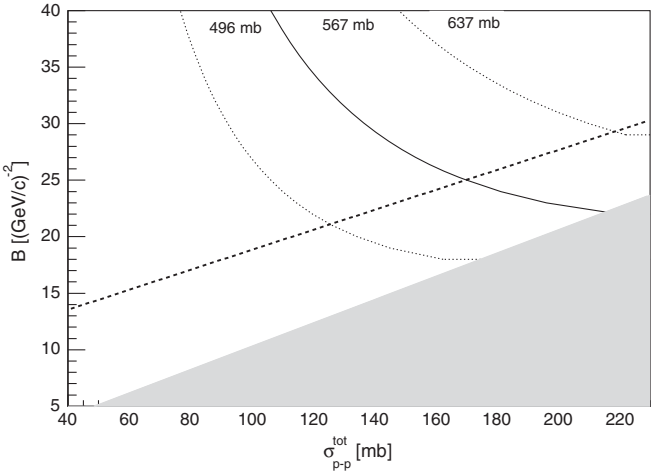

FIG. 8. The elastic slope B in $((\mathrm{GeV/c})^{-2})$ vs $\sigma^{\mathrm{total}}_{p-p}$ in mb. The solid and the dotted curves are the relation between B and $\sigma^{\mathrm{total}}_{p-p}$ for the constant value of the measured $\sigma^{\mathrm{inel}}_{p-\mathrm{air}}$ by the Telescope Array detector and the statistical error using Glauber Formalism. The dashed line is the BHS QCD inspired fit [8]. While the gray shaded area is the unitarity constraint.

included. This includes the statistical (outer/thinner error bar) and the systematic (inner/thicker error bar).

V. PROTON-PROTON CROSS SECTION

From the TA proton-air cross section result we can determine the total proton-proton cross section. The process of inferring σ_{p-p} from $\sigma^{\mathrm{inel}}_{p-\mathrm{air}}$ is described in details in [35], and [36].

The σ_{p-p} is calculated from the measured cross section, also known as the inelastic cross section $\sigma^{\mathrm{inel}}_{p-\mathrm{air}}$, using both Glauber Formalism [37] and the relation:

$$\sigma^{\mathrm{inel}}_{p-\mathrm{air}} = \sigma^{\mathrm{total}}_{p-\mathrm{air}} - \sigma^{\mathrm{el}}_{p-\mathrm{air}} - \sigma^{\mathrm{qel}}_{p-\mathrm{air}} \tag{3}$$

Where $\sigma^{\mathrm{total}}_{p-\mathrm{air}}$ is the total cross section, $\sigma^{\mathrm{el}}_{p-\mathrm{air}}$ is the elastic cross section and $\sigma^{\mathrm{qel}}_{p-\mathrm{air}}$ is the quasielastic cross section. The quasielastic cross section corresponds to scattering processes in which nuclear excitation occurs without particle production.

The relation between the $\sigma^{\mathrm{inel}}_{p-\mathrm{air}}$ and the σ_{p-p} is highly dependent on the forward scattering elastic slope B.

$$B = \frac{d}{dt}\left[\ln\frac{d\sigma^{\mathrm{el}}_{p-p}}{dt}\right]_{t=0} \tag{4}$$

This is shown in the B, $\sigma^{\mathrm{total}}_{p-p}$ plane in Fig. 8. Here the solid and dotted curves represent a constant value of $\sigma^{\mathrm{inel}}_{p-\mathrm{air}}$ that reflects the Telescope Array measured value and the statistical fluctuations.

There have been many theories predicting the relationship between B and σ_{p-p}. However many of these models either failed to describe the elastic scattering data, or the elastic slope energy dependence from the Tevatron ([35,38,39]). A more updated theory using the single pomeron exchange model while describing the Tevatron data correctly is not consistent with the Unitarity constraint ([35,40]). Here the unitarity constraint is shown by solid grey shaded area in Fig. 8. A more recent prediction is the BHS fit [5]. It is consistent with unitarity while using a QCD inspired fit to the pp and $\bar{p}p$ data from the Tevatron. The dashed line in Fig. 8 shows the BHS prediction. Here

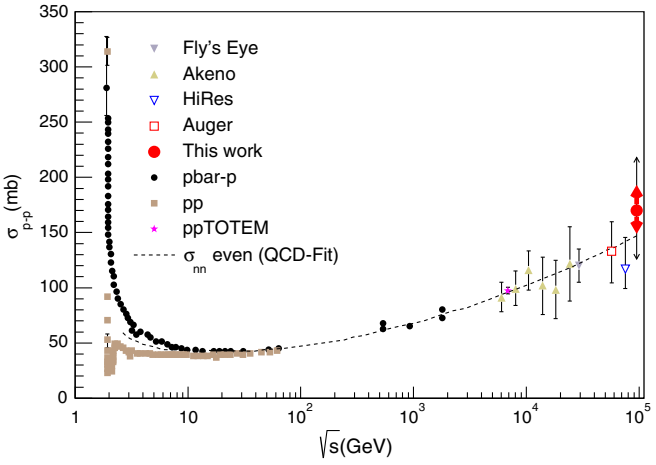

FIG. 9 (color online). The proton-proton cross section vs the center of mass energy result of this work, including the statistical (outer/thinner) and systematic (inner/thicker) error bars. The $\bar{p}p$ and the pp data are shown in smaller darker circles and square symbols consecutively [41]. The recent result from LHC is also shown by the star marker [42]. The result of this work is shown in comparison to previous work by cosmic rays detectors ([1,2,29,32]). The dashed curve is the QCD inspired fit by BHS [7].

$\sigma^{\text{inel}}_{p-\text{air}}$ is converted to $\sigma^{\text{total}}_{p-p}$ using the BHS fit. The statistical and systematic errors in $\sigma^{\text{total}}_{p-p}$ are propagated from the $\sigma^{\text{inel}}_{p-\text{air}}$ statistical and systematic error calculation. The $\sigma^{\text{total}}_{p-p}$ is found to be $170^{+48}_{-44}[\text{Stat}]^{+19}_{-17}[\text{Sys}]$ mb.

The $\sigma^{\text{total}}_{p-p}$ calculated in this work is shown in Fig. 9 compared to previous results from cosmic ray experiments like Fly's Eye [1], Akeno [29], HiRes [32], and Auger [2], together with accelerator pp and $\bar{p}p$ cross section measurement [41], in addition to the recent result from LHC by TOTEM [42]. The dotted curve is the QCD inspired fit of the total p-p cross section vs the center of mass energy $\sqrt{s}(\text{GeV})$ [7]. The result from this work at $\sqrt{s} = 95^{+5}_{-8}$ TeV, in addition to the most recent result published by the Auger experiment at $\sqrt{s} = 57$ TeV [2] and reported recent result by the LHC at $\sqrt{s} = 7$ TeV [42] are all in agreement with the fit.

VI. CONCLUSION AND OUTLOOK

In this work we used events collected by Telescope Array between May 2008 and May 2013 in hybrid mode to determine the $\sigma^{\text{inel}}_{p-\text{air}}$ using the K-factor method. The hadronic model dependence of the K-factor method was investigated. The latest updated hadronic interaction models have converged with time on the value of K with an uncertainty of $\sim 3\%$. This makes the K-factor method a weakly model dependent method to use in calculating the $\sigma^{\text{inel}}_{p-\text{air}}$. Several systematic checks were applied and the final value of $\sigma^{\text{inel}}_{p-\text{air}}$ was found to be equal to $567.0 \pm 70.5[\text{Stat}]^{+29}_{-25}[\text{Sys}]$ mb.

Ultimately the value of σ_{p-p} is determined from $\sigma^{\text{inel}}_{p-\text{air}}$ using Glauber theory and the BHS QCD inspired fit. Such a fundamental measurement at this high energy ($\sqrt{s} = 95^{+5}_{-8}$ TeV) could not be obtained with current particle accelerators. The value of $\sigma^{\text{tot}}_{p-p}$ was determined to be $170^{+48}_{-44}[\text{Stat}]^{+19}_{-17}[\text{Sys}]$ mb.

While the events used in this analysis were collected with the MD-SD part of the detector, future cross section results, using thoroughly analyzed events, could be performed using LR and BRM data and, ultimately, the full detector. LR and BRM are the FDs closer in distance to the SD and, therefore, we could extend the energy range of the collected data down to 1 EeV. This will enable us to study the measurement down to 1 EeV with higher statistical power which would allow us to constrain the available high-energy model cross section predictions.

ACKNOWLDGEMENTS

Many thanks to the CONEX and CORSIKA authors. Particular thanks to Tanguy Pierog for his help. The Telescope Array experiment is supported by the Japan Society for the Promotion of Science through Grants-in-Aid for Scientific Research on Specially Promoted Research (21000002) Extreme Phenomena in the Universe Explored by Highest Energy Cosmic Rays and for Scientific Research (19104006), and the Inter-University Research Program of the Institute for Cosmic Ray Research; by the U.S. National Science Foundation Awards No. PHY-0307098, No. PHY-0601915, No. PHY-0649681, No. PHY-0703893, No. PHY-0758342, No. PHY-0848320, No. PHY-1069280, No. PHY-1069286, No. PHY-1404495, and No. PHY-1404502; by the National Research Foundation of Korea (No. 2007-0093860, No. R32-10130, No. 2012R1A1A2008381, No. 2013004883); by the Russian Academy of Sciences, RFBR Grants No. 11-02-01528a and No. 13-02-01311a (I. N. R.), IISN Project No. 4.4502.13, and Belgian Science Policy under IUAP VII/37 (U. L. B.). The foundations of Dr. Ezekiel R. and Edna Wattis Dumke, Willard L. Eccles, and George S. and Dolores Doré Eccles all helped with generous donations. The State of Utah supported the project through its Economic Development Board, and the University of Utah through the Office of the Vice President for Research. The experimental site became available through the cooperation of the Utah School and Institutional Trust Lands Administration (SITLA), U.S. Bureau of Land Management, and the U.S. Air Force. We also wish to thank the people and the officials of Millard County, Utah, for their steadfast and warm support. We gratefully acknowledge the contributions from the technical staffs of our home institutions. An allocation of computer time from the Center for High Performance Computing at the University of Utah is gratefully acknowledged.

[1] R. M. Baltrusaitis, G. L. Cassiday, J. W. Elbert, P. R. Gerhardy, S. Ko, E. C. Loh, Y. Mizumoto, P. Sokolsky, and D. Steck, Phys. Rev. Lett. **52**, 1380 (1984).
[2] P. Abreu *et al.* (Pierre Auger Collaboration), Phys. Rev. Lett. **109**, 062002 (2012).
[3] R. Ulrich, R. Engel, and M. Unger, Phys. Rev. D **83**, 054026 (2011).
[4] R. Abbasi, M. Abe, T. Abu-Zayyad, M. Allen, R. Anderson *et al.*, Astropart. Phys. **64**, 49 (2015).
[5] M. Block, Phys. Rev. D **84**, 091501 (2011).
[6] M. M. Block, Phys. Rev. D **76**, 111503 (2007).
[7] M. Block and F. Halzen, Phys. Rev. D **72**, 036006 (2005).
[8] M. Block, F. Halzen, and T. Stanev, Phys. Rev. D **62**, 077501 (2000).

[9] T. Abu-Zayyad *et al.* (Telescope Array Collaboration), Nucl. Instrum. Methods Phys. Res., Sect A **689**, 87 (2012).
[10] H. Tokuno, Y. Tameda, M. Takeda, K. Kadota, D. Ikeda *et al.*, Nucl. Instrum. Methods Phys. Res., Sect. A **676**, 54 (2012).
[11] T. Bergmann, R. Engel, D. Heck, N. Kalmykov, S. Ostapchenko, T. Pierog, T. Thouw, and K. Werner, Astropart. Phys. **26**, 420 (2007).
[12] T. Pierog *et al.*, Nucl. Phys. B, Proc. Suppl. **151**, 159 (2006).
[13] G. Bossard, H. J. Drescher, N. N. Kalmykov, S. Ostapchenko, A. I. Pavlov, T. Pierog, E. A. Vishnevskaya, and K. Werner, Phys. Rev. D **63**, 054030 (2001).
[14] D. Heck, G. Schatz, T. Thouw, J. Knapp, and J. Capdevielle (1998).
[15] B. Stokes, R. Cady, D. Ivanov, J. Matthews, and G. Thomson, Astropart. Phys. **35**, 759 (2012).
[16] S. Ostapchenko, Nucl. Phys. B, Proc. Suppl. **151**, 143 (2006).
[17] N. Kalmykov, S. Ostapchenko, and A. Pavlov, Nucl. Phys. B, Proc. Suppl. **52**, 17 (1997).
[18] E.-J. Ahn, R. Engel, T. K. Gaisser, P. Lipari, and T. Stanev, Phys. Rev. D **80**, 094003 (2009).
[19] T. Pierog, I. Karpenko, J. Katzy, E. Yatsenko, and K. Werner, arXiv:1306.0121.
[20] C. Pryke, Astropart. Phys. **14**, 319 (2001).
[21] K. Greisen, Phys. Rev. Lett. **16**, 748 (1966).
[22] G. Zatsepin and V. Kuzmin, JETP Lett. **4**, 78 (1966).
[23] T. Abu-Zayyad *et al.* (Telescope Array Collaboration), Phys. Rev. D **88**, 112005 (2013).
[24] A. Glushkov, I. Makarov, M. Pravdin, I. Sleptsov, D. Gorbunov, G. Rubtsov, and S. Troitsky (Yakutsk EAS Array), Phys. Rev. D **82**, 041101 (2010).
[25] J. Abraham *et al.* (Pierre Auger Collaboration), Astropart. Phys. **31**, 399 (2009).
[26] M. Settimo (Pierre Auger), in International Cosmic Ray Conference.
[27] A. Aab *et al.* (Pierre Auger), Phys. Rev. D **90**, 122006 (2014).
[28] F. Siohan, R. W. Ellsworth, A. S. Ito, J. R. Macfall, R. E. Streitmatter, S. C. Tonwar, and G. B. Yodh, J. Phys. G **4**, 1169 (1978).
[29] M. Honda, M. Nagano, S. Tonwar, K. Kasahara, T. Hara, N. Hayashida, Y. Matsubara, M. Teshima, and S. Yoshida, Phys. Rev. Lett. **70**, 525 (1993).
[30] S. Knurenkoa, A. Sabourovb *et al.*, Eur. Phys. J. Conf. Abstr. **53**, 07006 (2013).
[31] H. Mielke, M. Foeller, J. Engler, and J. Knapp, J. Phys. G **20**, 637 (1994).
[32] K. Belov (HiRes Collaboration), Nucl. Phys. B, Proc. Suppl. **151**, 197 (2006).
[33] G. Aielli *et al.* (ARGO-YBJ Collaboration), Phys. Rev. D **80**, 092004 (2009).
[34] M. Aglietta *et al.* (EAS-TOP Collaboration), Phys. Rev. D **79**, 032004 (2009).
[35] R. Engel, T. Gaisser, P. Lipari, and T. Stanev, Phys. Rev. D **58**, 014019 (1998).
[36] T. Gaisser, U. Sukhatme, and G. Yodh, Phys. Rev. D **36**, 1350 (1987).
[37] R. Glauber and G. Matthiae, Nucl. Phys. **B21**, 135 (1970).
[38] J. Dias de Deus and P. Kroll, Acta Phys. Pol. B **9**, 157 (1978).
[39] A. Buras and J. Dias de Deus, Nucl. Phys. **B71**, 481 (1974).
[40] A. Donnachie and P. Landshoff, Phys. Lett. B **296**, 227 (1992).
[41] C. Avila *et al.*, Phys. Lett. B **445**, 419 (1999).
[42] G. Antchev, P. Aspell, I. Atanassov, V. Avati, J. Baechler *et al.*, Europhys. Lett. **96**, 21002 (2011).